Synthesis of Tellurium Fusiform Nanoarchitectures by Controlled Living Nanowire Modification

Yunpeng Zuo,[∥,†] Tingting Li,[∥,†] Dewei Rao,[∥,‡] Xiaomin Lei,[†] Qin Li,[†] Guilin Zhu,[†] Ruifeng Lu,[§] and Heyou Han*,[†]

[†]State Key Laboratory of Agricultural Microbiology, College of Science, Huazhong Agricultural University, Wuhan 430070, P. R. China
[‡]Institute for Advanced Materials, Jiangsu University, Zhenjiang 212013, P. R. China
[§]Department of Applied Physics, Nanjing University of Science and Technology, Nanjing 210094, P. R. China

Ⓢ Supporting Information

ABSTRACT: Control of structure-enriched abundant unsaturated or dangling bonds can precisely and effectively tune the activity and durability of materials. In this study, a new strategy to obtain fusiform nanoarchitectures (FNAs) has been found for the first time using Te nanostructures as the model materials. TeFNA could be transformed from Te nanorods (NRs) with different diameter (50, 25 nm), even the ultrathin nanowires (NWs) (10 nm). Besides, a novel perspective into the preliminary mechanism combining collision theory with density functional theory simulations was proposed to explain the transformation progress. In the mixing system of hexadecyl trimethylammonium bromide (CTAB) solution, the Te NR/NWs keep the translational motion together with the centroid rotation. The velocity of the two ends of TeNR/NWs is higher than that in the center under the reaction condition based on collision theory; meanwhile, the summation energy of both O_2 and CTAB put on Te (0001) surface is −606.992 eV, which means that the Te (0001) can be oxidized easily in the presence of CTAB. Moreover, this approach, which regulates the morphology of the existing structure, could provide a novel potential way to synthesize FNAs for their advanced functional applications.
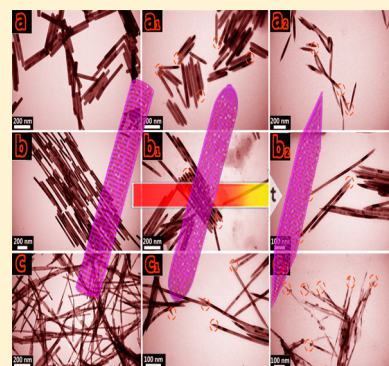
INTRODUCTION

Great progress has been made in the research on the surface structure of nanomaterial, including size, shape, and facets, in the past two decades.[1−3] Surfactants play an important role in the process that could obtain materials with more active surface areas or specific areas. Fusiform nanoarchitecture (FNA)-enriched abundant unsaturated or dangling bonds have attracted considerable attention as ideal structures for various applications.[1,3,4] Nanoproducts are also gradually applied in cancer treatment,[4,5] battery,[6] mobile client,[7] and so on. While surfactants are widely used in the synthesis and stabilization of nanomaterials,[8−10] the obtained nanomaterials could also be processed in the presence of surfactant under some conditions. Meanwhile, wide attention has recently been paid to Te nanostructures in organic and inorganic chemistry, which can reflect, at least in part, the huge application potential of the materials.[11,12] As a typical p-type semiconductor, Te has a higher hole carrier density than the electron concentration.[12] Additionally, Te has a narrow band gap (0.33 eV), implying that the wavelength limit of the optical sensor based on Te can reach the micron level. The attractive properties of tellurium indicate its potential use as template for synthesis of a series of metals (Au, Ag, Pt, Pd, Ni, etc.).[13−16] Previous studies clearly illustrate that Te nanomaterials are essential for materials science.

One-dimensional (1-D) FNA has attracted the attention of researchers in different fields including catalysis and photo-electricity,[17,18] owing to the advantages of their unique properties such as (1) stability of structure and perform-ance,[19,20] (2) lattice strain relaxation in heterojunction,[21] and (3) tunable optical resonances.[22] The properties of the nanomaterials could be controlled by morphology adjustment, but the difficulty lies in finding the appropriate methods to control their morphologies.[23] One of the difficulties of controlling the morphology of the Te arises from the anisotropic growth characteristics.[24] To date, various strategies have been developed to synthesize Te nanorods/wires, while there has been little research about the Te FNA.[25−27] CdTe nanocrystals were chosen as the precursor, Te nanocrystals were formed by air oxidation of CdTe nanocrystals, and, then, the spherical Te nanocrystals grew into nanorods/nanowires and finally generated the double-directional nanoneedles with sharp tips;[28] however, the tedious reaction steps and complex synthesis conditions both limited the use of Te FNA. In this paper, a new strategy to obtain Te FNA was created by controlling the living 1D nanostructure modification. The
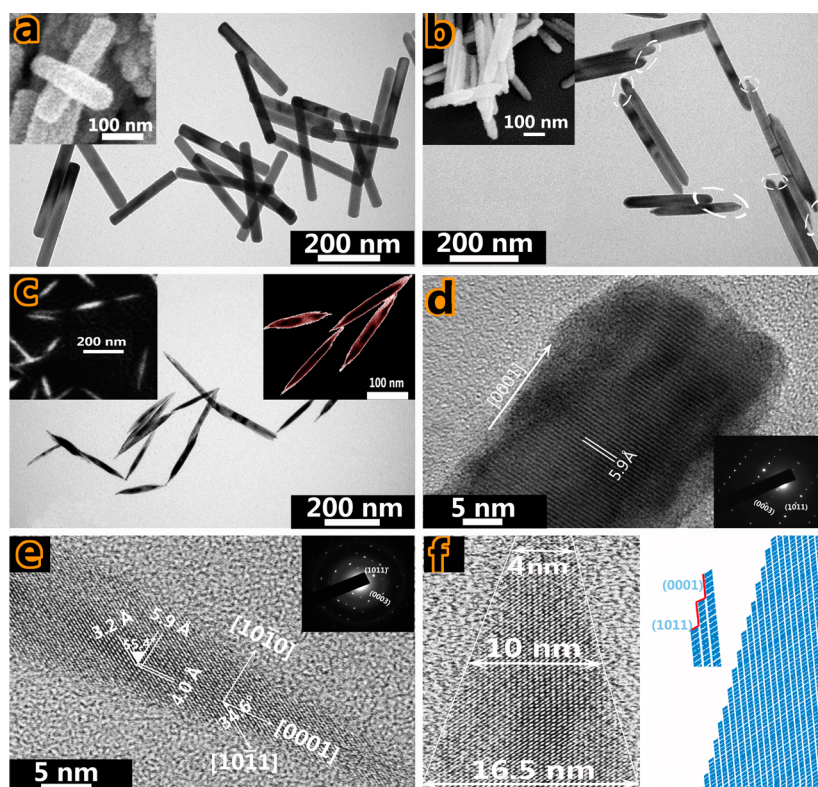
Figure 1. (a) TEM image and FESEM image (inset in panel a) of the TeNRs, (b,c) TEM and FESEM images (insets in the upper right corner of panels b and c) of the evolution from TeNRs to TeNFs with well-defined morphologies and enlarged TEM image embedded in the upper right corner of panel c. (d,e) HRTEM images of the TeNRs, TeNFs, and SAED patterns (insets in panels d and e) of the square area. (f) Enlarged HRTEM image (f1, left) taken from the sharp edges of a fusiform architecture and illustration (f1, right) of the atomic arrangement on the {0001} surface.

whole process has relatively simple setups and procedures that can obtain Te FNA with different diameters or lengths with the change of Te precursor nanostructures. This protocol provides a new general route for the controllable synthesis of sharp tips structure.

■ EXPERIMENTAL SECTION

Methods and Apparatus. In the present study, the Te nanofusiform structures (TeNFs) were synthesized for the first time from Te nanorods (TeNRs) in the presence of CTAB, while the structure of TeNRs almost did not change in the absence of CTAB. The Te nanomaterials used in the experiments were synthesized as reported in our previous work.[10] Additionally, in this study, the effects of CTAB on the transformation of TeNRs into TeNFs were investigated from the viewpoint of reaction kinetics. Absorption measurements were performed with a UV−vis−NIR spectrophotometer to confirm the optical nature of Te nanomaterials.

Transmission electron microscopy (TEM) and high-resolution transmission electron microscopy (HRTEM) measurements were made on a JEM-2010FEF high-resolution transmission electron microscope at an accelerating voltage of 200 kV. The X-ray diffraction (XRD) analysis was carried out on a Bruker D8 Advance X-ray diffractometer with Cu Kα radiation. Absorption measurements were performed with a UV−vis-NIR spectrophotometer (PerkinElmer Lambda 750).

Preparation of TeNRs with the Diameter Close to 50 nm. In a typical synthesis, 6 mL of $N_2H_4 \cdot H_2O$ was quickly added to a reaction bottle with TeO_2 powder (35 mg) at 60 °C under constant magnetic stirring. With the color of the solution

gradually changed into blue gray after 10 min, the special TeNRs were obtained. Then, the mixture should dilute 10-fold with sodium dodecyl sulfonate (SDS, 10 mM) to obtain well-defined TeNRs, and the products were subjected to a centrifugation/wash cycle to remove most of the matrices, including SDS and hydrazine. Finally, as-prepared TeNRs were dispersed in 10 mL of water.

Preparation of TeNRs with the Diameter Close to 25 nm. In this process of synthesis, 8 mL of $N_2H_4 \cdot H_2O$ was added to the reaction bottle with TeO_2 powder (30 mg) at 30 °C under constant magnetic stirring. The color of the solution gradually changed to blue after 15 min; then, the products were processed according to the above method just as the synthesis of TeNRs (50 nm).

Synthesis of TeNWs with the Diameter Close to 10 nm. Ten milliliters of $N_2H_4 \cdot H_2O$ was added to the reaction bottle with TeO_2 powder (30 mg) at 30 °C under constant magnetic stirring. The color of the solution gradually changed to blue after 30 min; then, the products were processed according to the above method just as the synthesis of TeNRs (50 nm).

Synthesis of TeNFs. One milliliter of as-prepared TeNR/NWs subjected to centrifugation/wash one time was dispersed in 10 mL of CTAB solution (27.5 mM) under constant magnetic stirring at 60 °C for 90 min. The TeNFs were obtained after a centrifugation/wash cycle to remove most of the matrices.

Density Functional Theory Calculations. All calculations in this work were performed using Vienna Ab-initio Simulation Package.[29] The ion−electron interaction is described with the

projected augmented wave method, and the exchange-correlation functional is Perdew—Burke—Ernzerhof in the generalized gradient approximation.[30−32] Numerical calculations were accomplished with the following criterions: The convergence thresholds are set to 10^{-5} eV in energy and 10^{-2} eV/Å in force with the cutoff energy of 500 eV. More details of the density functional theory (DFT) calculations are described in the Supporting Information (Table S1 and Figure S1).

■ RESULTS AND DISCUSSION

Figure 1 shows the TEM and field-emission scanning electron microscopy (FESEM) images of Te nanostructures. The as-prepared TeNRs are highly uniform with a narrow diameter distribution of ∼60 nm, as shown in Figure 1a. The d spacing of adjacent fringes for the TeNRs is 5.9 Å (Figure 1d), which can be attributed to (0001) facets.[33] Figure 1b,c and Figure S2 clearly show the evolution of TeNRs to TeNFs. Moreover, the FESEM images embedded in the upper left corner in Figure 1a−c further confirm the above conclusions. The obtained TeNFs with a well-defined fusiform structure have two highly sharp edges. The crystal structure in the chemical progress changed and produced crystal faces with more edge and corner atoms, which could be verified from SAED patterns (insets in panels d an e) of the square area and enlarged HRTEM image (f1, left) taken from the sharp edges of a fusiform structure and illustration (f1, right) of the atomic arrangement on the {0001} surface.

Oxygen plays an important role in the corrosion of Te nanomaterials in water solution;[16] however, the TeNFs could only be obtained from TeNRs in the presence of CTAB, while the morphology of TeNRs almost did not change in the absence of CTAB. Moreover, there was little difference in the change of the structure of TeNRs under oxygen- and nitrogen-saturated conditions, as shown in Figure S3, revealing that CTAB can accelerate the reaction rate and play the role of catalyst. In the mixing system of CTAB solution, the colloidal and dissolved oxygen molecules are homogeneously dispersed in the solution in the case of high-speed agitation, the kinestate of TeNRs including the overall translational motion form, and the centroid rotation, as shown in Scheme 1.[34] For the overall translational motion, the speed of various parts of TeNRs is identical (Scheme 1b$_{(1)}$, $v_1 = v_2 = v_3$) under the constant magnetic stirring, and the collision probability between various parts of TeNRs and colloid and oxygen molecules is the same under the overall translational motion form.[35] On the basis of the Arrhenius mode of expansion exponential type, as shown in eq 1,[35] κ is the rate constant, R is a constant of molar gas, T is the thermodynamic temperature, and β is a dimensionless quantity

$$\kappa = A e^{\left[-\left(\frac{E_\alpha}{RT}\right)^\beta\right]}$$

(1)

The activation energy (E_α) of the reaction is fixed in a certain solution and temperature, and thus the frequency factor (A) will determine the rate of the reaction, and the A is positively related to the number of effective collisions.[16,35] Therefore, the reaction rate of the various parts of the TeNRs is the same, inducing the diminution of TeNRs tend to be occurred. On the contrary, the velocity of two ends of TeNRs (v_1, v_3) is higher than that in the center (v_2) under the mass-center motions form (Scheme 1b$_{(2)①,(2)②}$).[34] The direction of mass-center rotation will reverse spontaneously sometimes. Moreover, the
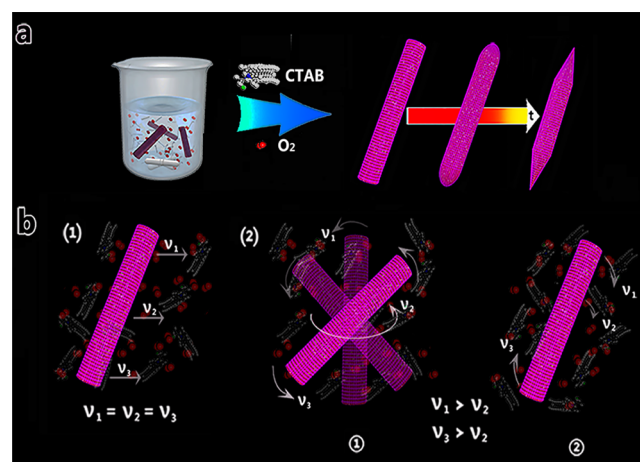
Scheme 1[a]

[a](a) Simulation of the growth process from TeNRs to TeNFs corresponding to TEM images for different periods of reaction. Schematic illustration of (b) two different kinestates of the TeNRs in the CTAB solution including (b$_{(1)}$) the overall translational motion form and (b$_{(2)}$) the two forms of rotation around the centroid (b$_{(2)①}$) and (b$_{(2)②}$).

period of rotation motion at the two ends is identical to that of the centroid rotation of the central part of TeNRs. The collision probability between the two ends of the TeNRs and the colloidal molecules and the dissolved oxygen molecules is greater than that of central part, leading to more rapid reaction of the ends of the TeNRs and facilitating the formation of the fusiform structure of TeNFs.[34,35] Taken together, the Te nanomaterials keep the translational motion together with the centroid rotation under constant magnetic stirring for several tens of minutes in the CTAB solution, resulting in the diminution of 1D Te nanostructures and the formation of certain FNAs in the presence of CTAB, as shown in Scheme 1a.

To further validate the applicability of the above-mentioned factors, we performed DFT calculations to obtain the total energy for the possible reaction pathways as follows: including (1) isolated O_2, CTAB, and Te (0001), (2) O_2 combined with Te (0001) surface (OT), plus CTAB, (3) O_2 sited on CTAB (OC), plus Te (0001), and (4) both O_2 and CTAB on Te (0001) surface (OCT). All calculated data are displayed in Table S2. The sum energy of O_2 and Te (0001) is −267.537 eV, lower than the total energy of OT (−258.848 eV), which means that the Te (0001) is difficult to be oxidized without providing extra energy. In the case of the introduction of CTAB, the summation energy of O_2, CTAB, and Te (0001) is −605.447 eV, higher than the summation energy of Te (0001) and OC (−605.838 eV) as well as the energy of OCT (−606.992 eV), which means that the Te (0001) can be oxidized easily in the presence of CTAB. A detailed comparison is shown in Scheme 2 with the total energies of O_2, CTAB, and Te (0001) as the benchmark (0 eV). The relative energies of the other states are shown in Scheme 2 (2, 3, 4). Moreover, Te fusiform structures cannot form from nanorods in the sodium dodecyl sulfates solution as well as in the bromide ion solution. Figure S4 shows the TEM images of Te nanoarchitectures under different conditions. Thus, the cationic groups in CTAB might play a significant role in the reaction. Our DFT calculations demonstrate the significant catalysis of CTAB for Te reacted with O_2.

Scheme 2. DFT Calculations of the Total Energy for (1) Isolated O_2, CTAB, and Te (0001), (2) O_2 Combined with Te (0001) Surface (OT), Plus CTAB, (3) O_2 Sited on CTAB (OC), Plus Te (0001), and (4) Both O_2 and CTAB on Te (0001) Surface (OCT)
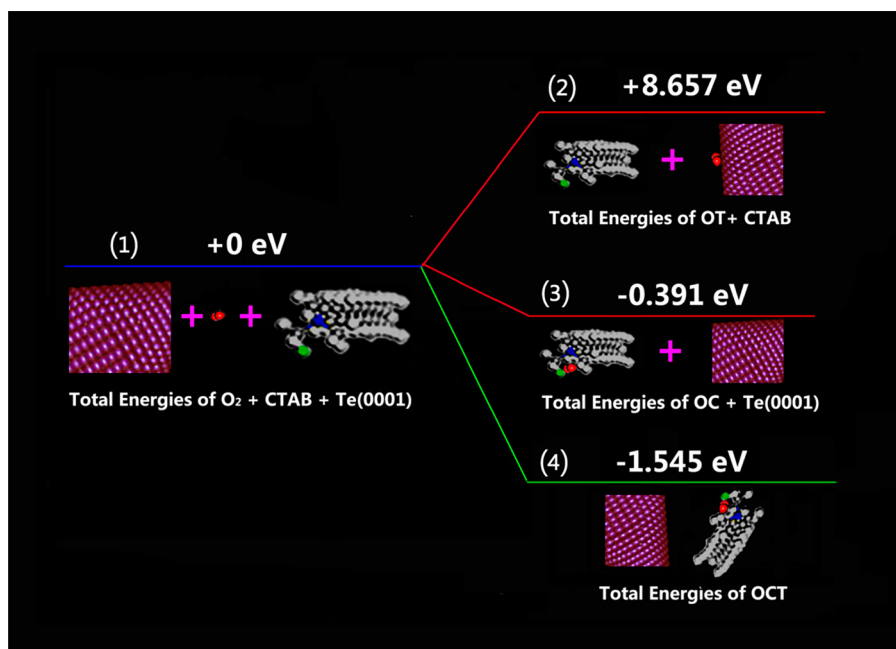
The above conclusion was established based on the dependence of related factors on the stirring rates of the reaction because the stirring rate is positively related to the A variable in eq 1. Therefore, different constant magnetic stirring rates (0, 400, 800, 1200 r/min) were set to regulate and control the collision rates between the various parts of TeNRs and colloids and the dissolved oxygen molecules.[34] When the stirring rate is reduced, the translational rate of the rod is smaller, and the reaction of the process will be slower. Meanwhile, the rotation rate of the TeNRs as well as the collision probability between the reactants will also be declined.[34,35] The structure of TeNRs almost did not change after 110 min under 0 r/min at 60 °C, as shown in Figure S5. Figure S6 and Figure 2 show the TEM about morphology transformation of Te nanomaterials under different stirring speeds. Figure 2a,a₁ shows the TEM images of Te nanomaterials at different reaction time. With increasing stirring speed, the rate of the reaction is also increasing, and the diameter of the TeNFs gradually becomes smaller (Figure 2a₁−c₁). The results are consistent with the above conclusion. The XRD pattern of Te nanostructures in Figure 3a shows that all peaks can be indexed to hexagonal crystal system Te, which is consistent with the standard literature values (JCPDF no. 36-1452).[34] As the structure of the TeNRs gradually changed into TeNFs, {0001} became the advantage exposed facet, while the absorption peak in XRD spectra decreased, which might indicate the continuous decrease in the crystallinity of the nanomaterials.[35] To further verify the change of the structure, we studied Raman spectra of the synthesized Te nanostructures, and the result is shown in Figure 3b. The decrease in the intensity shown in Figure 3b might be caused by the change of the structure.[33,36−38] Overall, the analyses of XRD and Raman spectra were consistent with the changes of Te nanostructures from rod to fusiform.

A number of empirical factors were investigated to confirm the interdependency of the CTAB and Te systems. The
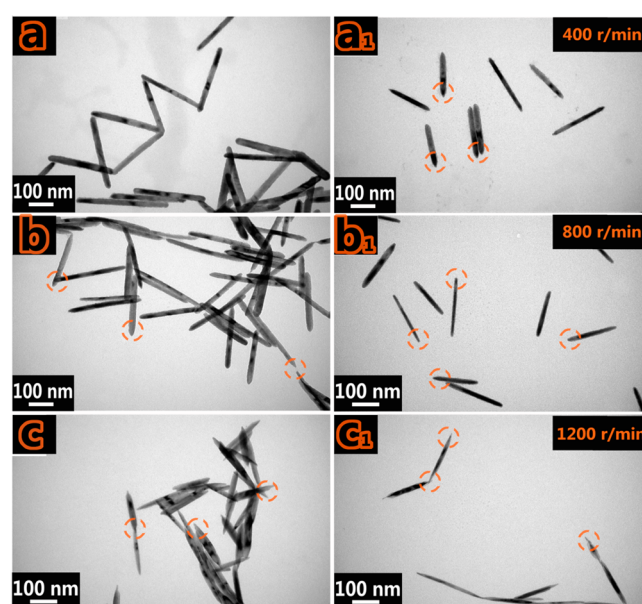

Figure 2. TEM image of the TeNRs and corresponding TEM images of the samples obtained at three representative stirring rates (a,a₁) 400, (b,b₁) 800, and (c,c₁) 1200 r/min during the evolution process from 1D Te NR/NWs to nanofusiforms.

concentration gradients of CTAB (0, 13.7, 27.5, 41.2, 54.9 mM) were observed, and the process was characterized by absorption spectra. Figure S7 shows the UV spectra of the reaction corresponding to the change of nanostructures from rod to fusiform. With the continuous sharpening of both the rod ends, the longitudinal absorption peak position gradually becomes larger, while the lateral absorption peak gradually grows smaller, as shown in Figure S8. When the concentration of CTAB is 27.5 mM, the structural alteration of Te is very obvious, which is consistent with the TEM images in Figure 1.
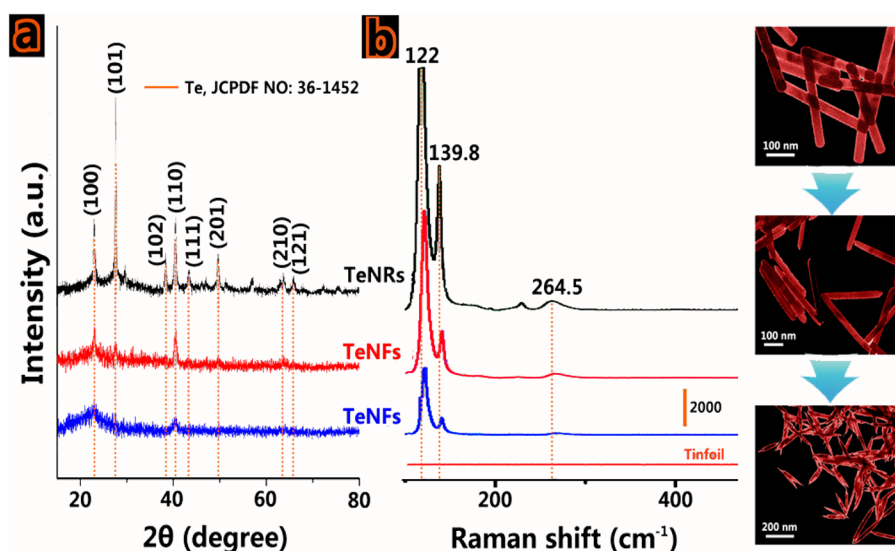
Figure 3. (a) X-ray diffraction (XRD) pattern and (b) Raman spectra of Te nanostructures transformed from rod to fusiform with the TEM images embedded (from top to bottom).
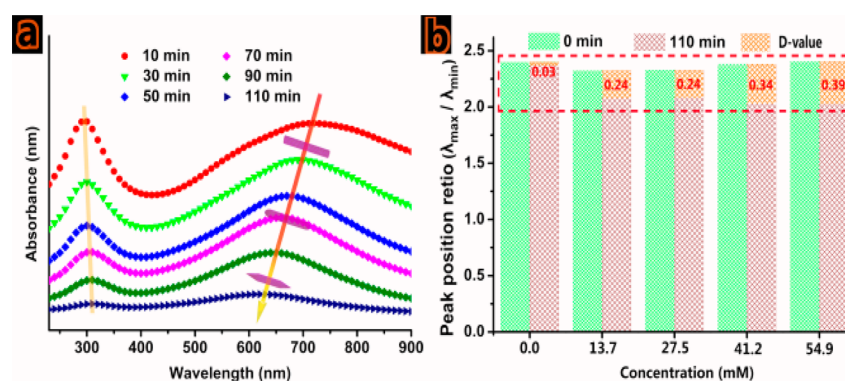
Figure 4. (a) Changes in absorption spectra of substrate with catalytic time of 0, 10, 30, 50, 70, 90, 110, and 130 min (from top to bottom) under CTAB concentration of 27.5 mM. (b) Difference values of the peak-position ratio ($\lambda_{max}/\lambda_{min}$) of each CTAB concentration point (0, 13.7, 27.5, 41.2, 54.9 mM) between 0 and 110 min are 0.03, 0.24, 0.24, 0.34, 0.39.

Optical measurements on Te nanomaterial (with the concentration of CTAB is 27.5 mM) ensembles confirm the gradual decrease in the absorption peak of Te and the decrease in the size when the reaction proceeded, as shown in Figure 4a. According to the Hartree−Fock−Slater study,[39−41] the minimum absorption peak (λ_{min} in the range of 260−300 nm) might be caused by the transition from the valence band (p-bonding VB2) to the conduction band (p-antibonding CB1), and the maximum absorption peak (λ_{max} in the range of 600−900 nm) might be due to the transition from the valence band (p-lone-pair VB3) to p-antibonding CB1.[39−41] Moreover, with the structure change of the Te, the alteration of λ_{min} is far lower than that of λ_{max}, which means the aspect ratio (R) of TeNRs is associated with λ_{max}. On the basis of a previous study,[42,43] the derived relationship between the λ_{max} and R could be approximated with the introduction of the normalized variable η, as shown in the Supporting Information. As stated above, the peak-position ratio (ppR) of $\lambda_{max}/\lambda_{min}$ could be used to model the size change of Te nanostructure. The $\lambda_{max}/\lambda_{min}$ in Figure 4b and TEM analysis indicate the concentration of CTAB (27.5 mM) is suitable for the research. The difference value (D value) of the ppR of each CTAB concentration point (0, 13.7, 27.5, 41.2, 54.9 mM) between 0 and 110 min is 0.03,

0.24, 0.24, 0.34, and 0.39. For the given ppR, the dramatic changes in D value indicate a greater deviation from normality in the presence of CTAB, which further confirms that CTAB can accelerate the reaction rate and play the role of catalyst.

To further verify the above conclusion, we tested 1D Te nanomaterials with different diameter sizes and lengths in the same system for reaction. Here the morphology transformations of 1D Te nanostructures were measured with TEM. From Figure 5, we can see the well-defined taper change for TeNRs with a diameter close to 50 and 25 nm and ultrathin Te nanowires with a diameter close to 10 nm in the corresponding TEM images of the samples obtained at three representative stages during the evolution process from nanorods or nanowires to fusiform architecture. Figure 5a−c and Figure 5a₁−c₁ display the changes from initial 1D TeNRs/ wires to the intermediates of the 1D Te nanofusiform architectures, and Figure 5a₂−c₂ exhibits the final obtained 1D Te nanofusiform structures. TEM results are consistent with the principles illustrated in Scheme 1a.

■ CONCLUSIONS

We have found for the first time that TeNFs can be obtained by 1D TeNR/NWs in CTAB solution. The fusiform structures
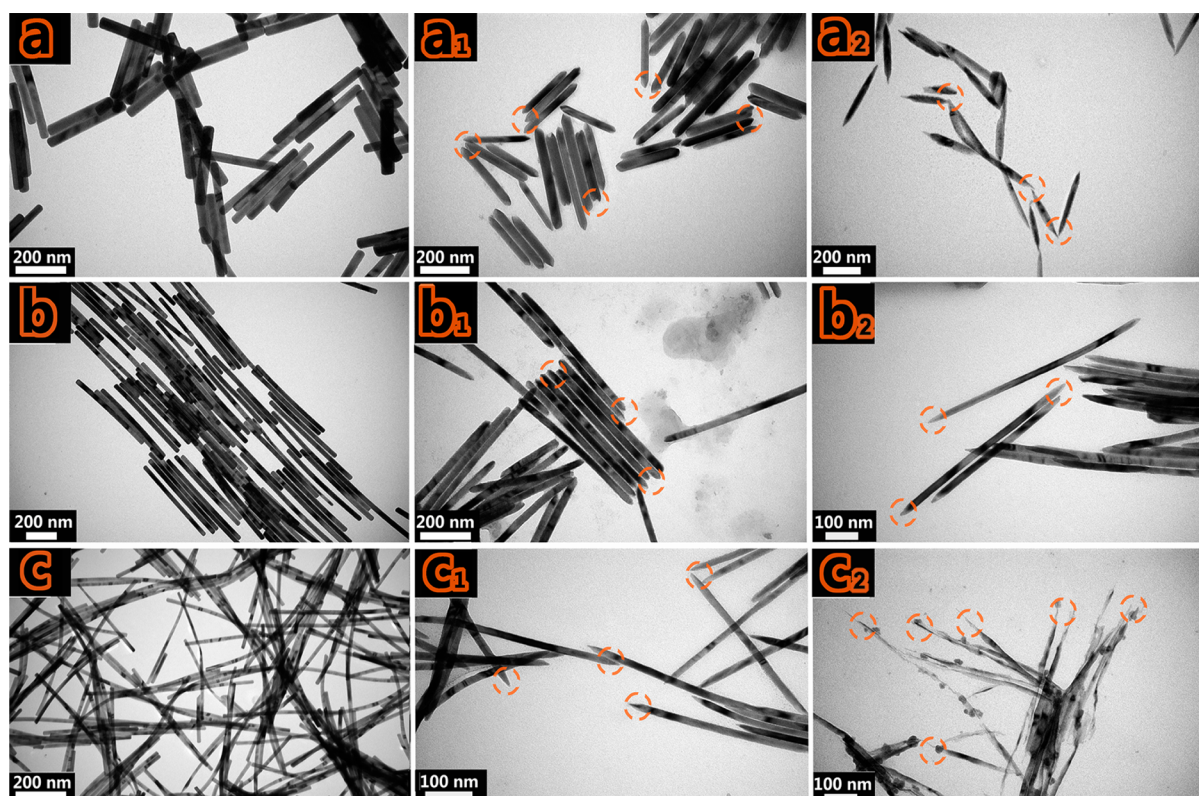
Figure 5. Well-defined taper change for Te nanorods with a different diameter close to 50 and 25 nm and ultrathin Te nanowires with a diameter close to 10 nm and corresponding TEM images of the samples obtained at three representative stages during the evolution process from nanorods or nanowires to fusiform architecture. (a−c) Initial 1D Te nanorods/wires. (a_1−c_1) 1D Te nanofusiform architecture intermediates. (a_2−c_2) Final 1D Te nanofusiform strucutres.

enriched large numbers of edge and corner atoms, which can be used to improve the potential applications of Te nanomaterials in various fields, such as synthesis of other noble metals/alloys and optoelectronic devices. A novel perspective into the preliminary mechanism was proposed to explain the transformation progress combined practical experiment with DFT calculations using 1D Te NR/NWs as the initial reactant. This transformation process could be described as follows: (1) In the mixing system of CTAB solution, the Te nanomaterials hold the translational motion together with the centroid rotation. (2) The reaction rate of the various parts of the TeNR/NWs is identical and the diminution of TeNRs tends to occur under the translational motion. (3) The velocity of the two ends of TeNR/NWs is higher than that in the center under the mass-center motion. The DFT calculations indicate the significant catalysis of CTAB for Te reacted with O_2. Collectively, the reaction is more rapid at the two ends of TeNR/NWs, which facilitates the formation of the fusiform structures of TeNFs.

ASSOCIATED CONTENT

Ⓢ Supporting Information

The Supporting Information is available free of charge on the ACS Publications website at DOI: 10.1021/acs.jpcc.6b03730.

Experimental details. Figure S1. Cluster models in present work. Figure S2. FESEM images of TeNRs, Te nano-intermediate substance, and TeNFs. Figure S3. TEM images of TeNRs. TEM images of the structure of TeNRs under oxygen and nitrogen-saturated conditions at 60 °C with constant magnetic stirring. Figure S4. TEM images of Te nano-architectures before and after dispersed in 10 mL SDS solution at 60 °C for 110 min under constant magnetic stirring. Figure S5. TEM images of TeNRs. TEM images of TeNRs after 110 min dispersed in 10 mL H_2O at 60 °C under constant magnetic stirring. Figure S6. TEM image of TeNRs. Figure S7. Changes in absorption spectra of substrate under different CTAB concentrations. Figure S8. Change of longitudinal absorption peak position (λ_{max}) and lateral absorption peak (λ_{min}) under different CTAB concentrations. Table S1. Lattice constants for each model. Table S2. The calculated data of the total energy for the several representative states. (PDF)

AUTHOR INFORMATION

Corresponding Author
*E-mail: hyhan@mail.hzau.edu.cn.

Author Contributions
‖Y.Z., T.L., and D.R. contributed equally to this work.

Notes
The authors declare no competing financial interest.

REFERENCES

(1) Zhu, C.; Du, D.; Eychmuller, A.; Lin, Y. Engineering Ordered and Nonordered Porous Noble Metal Nanostructures: Synthesis, Assembly, and Their Applications in Electrochemistry. *Chem. Rev.* **2015**, *115*, 8896−8943.

(2) Chen, C.; Kang, Y.; Huo, Z.; Zhu, Z.; Huang, W.; Xin, H. L.; Snyder, J. D.; Li, D.; Herron, J. A.; Mavrikakis, M.; et al. Highly Crystalline Multimetallic Nanoframes with Three-Dimensional Electrocatalytic Surfaces. *Science* **2014**, *343*, 1339−1343.

(3) Feld, A.; Merkl, J.-P.; Kloust, H.; Flessau, S.; Schmidtke, C.; Wolter, C.; Ostermann, J.; Kampferbeck, M.; Eggers, R.; Mews, A.; et al. A Universal Approach to Ultrasmall Magneto-Fluorescent Nanohybrids. *Angew. Chem., Int. Ed.* **2015**, *54*, 12468−12471.

(4) Wang, S.; Kim, G.; Lee, Y.-E. K.; Hah, H. J.; Ethirajan, M.; Pandey, R. K.; Kopelman, R. Multifunctional Biodegradable Polyacrylamide Nanocarriers for Cancer Theranostics—A"See and Treat" Strategy. *ACS Nano* **2012**, *6*, 6843−6851.

(5) Ayala-Orozco, C.; Urban, C.; Knight, M. W.; Urban, A. S.; Neumann, O.; Bishnoi, S. W.; Mukherjee, S.; Goodman, A. M.; Charron, H.; Mitchell, T.; et al. Au Nanomatryoshkas as Efficient Near-Infrared Phototermal Transducers for Cancer Treatment: Benchmarking against Nanoshells. *ACS Nano* **2014**, *8*, 6372−6381.

(6) Zhao, J.; Lu, Z.; Wang, H.; Liu, W.; Lee, H.; Yan, K.; Zhuo, D.; Lin, D.; Liu, N.; Cui, Y. Artificial Solid Electrolyte Interphase-Protected LixSi Nanoparticles: An Efficient and Stable Prelithiation Reagent for Lithium-Ion Batteries. *J. Am. Chem. Soc.* **2015**, *137*, 8372−8375.

(7) Zuo, Y.; Cai, K.; Wu, L.; Li, T.; Lv, Z.; Liu, J.; Shao, K.; Han, H. Spiny-Porous Platinum Nanotubes with Enhanced Electrocatalytic Activity for Methanol Oxidation. *J. Mater. Chem. A* **2015**, *3*, 1388−1391.

(8) Brege, J. J.; Hamilton, C. E.; Crouse, C. A.; Barron, A. R. Ultrasmall Copper Nanoparticles From A Hydrophobically Immobilized Surfactant Template. *Nano Lett.* **2009**, *9*, 2239−2242.

(9) Zheng, Z.; Tachikawa, T.; Majima, T. Single-Particle Study of Pt-Modified Au Nanorods for Plasmon-Enhanced Hydrogen Generation in Visible to Near-Infrared Region. *J. Am. Chem. Soc.* **2014**, *136*, 6870−6873.

(10) Zuo, Y.; Wu, L.; Cai, K.; Li, T.; Yin, W.; Li, D.; Li, N.; Liu, J.; Han, H. Platinum Dendritic-Flowers Prepared by Tellurium Nanowires Exhibit High Electrocatalytic Activity for Glycerol Oxidation. *ACS Appl. Mater. Interfaces* **2015**, *7*, 17725−17730.

(11) Wang, Q.; Safdar, M.; Xu, K.; Mirza, M.; Wang, Z.; He, J. Van der Waals Epitaxy and Photoresponse of Hexagonal Tellurium Nanoplates on Flexible Mica Sheets. *ACS Nano* **2014**, *8*, 7497−7505.

(12) Chivers, T.; Laitinen, R. S. Tellurium: A Maverick Among The Chalcogens. *Chem. Soc. Rev.* **2015**, *44*, 1725−1739.

(13) Zhu, C.; Guo, S.; Dong, S. PdM (M= Pt, Au) Bimetallic Alloy Nanowires with Enhanced Electrocatalytic Activity for Electro-Oxidation of Small Molecules. *Adv. Mater.* **2012**, *24*, 2326−2331.

(14) Li, H.; Ma, S.; Fu, Q.; Liu, X.; Wu, L.; Yu, S.-H. Scalable Bromide-Triggered Synthesis of Pd@ Pt Core-Shell Ultrathin Nanowires with Enhanced Electrocatalytic Performance toward Oxygen Reduction Reaction. *J. Am. Chem. Soc.* **2015**, *137*, 7862−7868.

(15) Li, H. H.; Zhao, S.; Gong, M.; Cui, C. H.; He, D.; Liang, H. W.; Wu, L.; Yu, S.-H. Ultrathin PtPdTe Nanowires As Superior Catalysts for Methanol Electrooxidation. *Angew. Chem., Int. Ed.* **2013**, *52*, 7472−7476.

(16) Xu, L.; Liang, H.-W.; Li, H.-H.; Wang, K.; Yang, Y.; Song, L.; Wang, X.; Yu, S.-H. Understanding The Stability and Reactivity of Ultrathin Tellurium Nanowires In Solution: An Emerging Platform for Chemical Transformation and Material Design. *Nano Res.* **2015**, *8*, 1081−1097.

(17) Alia, S. M.; Zhang, G.; Kisailus, D.; Li, D.; Gu, S.; Jensen, K.; Yan, Y. Porous Platinum Nanotubes for Oxygen Reduction and Methanol Oxidation Reactions. *Adv. Funct. Mater.* **2010**, *20*, 3742−3746.

(18) Yang, H.; Finefrock, S. W.; Albarracin Caballero, J. D.; Wu, Y. Environmentally Benign Synthesis of Ultrathin Metal Telluride Nanowires. *J. Am. Chem. Soc.* **2014**, *136*, 10242−10245.

(19) Alia, S. M.; Jensen, K.; Contreras, C.; Garzon, F.; Pivovar, B.; Yan, Y. Platinum Coated Copper Nanowires and Platinum Nanotubes as Oxygen Reduction Electrocatalysts. *ACS Catal.* **2013**, *3*, 358−362.

(20) Xia, B.; Wu, H.; Yan, Y.; Lou, X.-W.; Wang, X. Ultrathin and Ultralong Single-Crystal Platinum Nanowire Assemblies with Highly Stable Electrocatalytic Activity. *J. Am. Chem. Soc.* **2013**, *135*, 9480−9485.

(21) Hauenstein, R. J.; Clemens, B. M.; Miles, R. H.; Marsh, O. J.; Croke, E. T.; McGill, T. C. Strain Relaxation Kinetics in Si$_{1−x}$Gex/Si Heterostructures. *J. Vac. Sci. Technol., B: Microelectron. Process. Phenom.* **1989**, *7*, 767−774.

(22) Dorfmüller, J.; Vogelgesang, R.; Weitz, R. T.; Rockstuhl, C.; Etrich, C.; Pertsch, T.; Lederer, F.; Kern, K. Fabry-Pérot Resonances in One-Dimensional Plasmonic Nanostructures. *Nano Lett.* **2009**, *9*, 2372−2377.

(23) Zhang, H.; Jin, M.; Xia, Y. Noble-Metal Nanocrystals with Concave Surfaces: Synthesis and Applications. *Angew. Chem., Int. Ed.* **2012**, *51*, 7656−7673.

(24) Zhu, H.; Zhang, H.; Liang, J.; Rao, G.; Li, J.; Liu, G.; Du, Z.; Fan, H.; Luo, J. Controlled Synthesis of Tellurium Nanostructures from Nanotubes to Nanorods and Nanowires and Their Template Applications. *J. Phys. Chem. C* **2011**, *115*, 6375−6380.

(25) Yang, Y.; Wang, K.; Liang, H.; Liu, G.; Feng, M.; Xu, L.; Liu, J.; Wang, J.; Yu, S. H. A New Generation of Alloyed/ Multimetal Chalcogenide Nanowires by Chemical Transformation. *Sci. Adv.* **2015**, *1*, e1500714.

(26) Wang, K.; Yang, Y.; Liang, H.; Liu, J.; Yu, S. H. First Sub-Kilogram-Scale Synthesis of High Quality Ultrathin Tellurium Nanowires. *Mater. Horiz.* **2014**, *1*, 338−343.

(27) Liu, J.; Xu, J.; Hu, W.; Yang, J.; Yu, S. H. Systematic Synthesis of Tellurium Nanostructures and Their Optical Properties: From Nanoparticles to Nanorods, Nanowires, and Nanotubes. *ChemNanoMat* **2016**, *2*, 167−170.

(28) Deng, Z.; Chen, D.; Tang, F.; Mansuripur, M. Growth of Single-Crystal Double-Directional Tellurium Nanoneedles from CdTe Nanocrystals in Solution. *Cryst. Growth Des.* **2009**, *9*, 1823−1828.

(29) Kresse, G.; Furthmuller, J. Efficient Iterative Schemes for Abinitio Total-Energy Calculations Using A Plane-Wave Basis Set. *Phys. Rev. B: Condens. Matter Mater. Phys.* **1996**, *54*, 11169−11186.

(30) Blöchl, P. E. Projector Augmented-Wave Method. *Phys. Rev. B: Condens. Matter Mater. Phys.* **1994**, *50*, 17953−79.

(31) kresse, G.; Joubert, D. From Ultrasoft Pseudopotentials to The Projector Augmented-Wave Method. *Phys. Rev. B: Condens. Matter Mater. Phys.* **1999**, *59*, 1758−75.

(32) Papavassiliou, G. C. Optical Properties of Small Inorganic and Organic Metal Particles. *Prog. Solid State Chem.* **1979**, *12*, 185.

(33) Fu, S.; Cai, K.; Wu, L.; Han, H. One-Step Synthesis of High-Quality Homogenous Te/Se Alloy Nanorods with Various Morphologies. *CrystEngComm* **2015**, *17*, 3243−3250.

(34) Qian, H.-S.; Yu, S.-H.; Gong, J.-Y.; Luo, L.-B.; Fei, L.-F. High-Quality Luminescent Tellurium Nanowires of Several Nanometers in Diameter and High Aspect Ratio Synthesized by a Poly (Vinyl Pyrrolidone)-Assisted Hydrothermal Process. *Langmuir* **2006**, *22*, 3830−3835.

(35) Wang, H.; Cui, L.-F.; Yang, Y.; Sanchez Casalongue, H.; Robinson, J. T.; Liang, Y.; Cui, Y.; Dai, H. Mn$_3$O$_4$− Graphene Hybrid as a High-Capacity Anode Material for Lithium ion Batteries. *J. Am. Chem. Soc.* **2010**, *132*, 13978−13980.

(36) Shao, F.; Lu, Z.; Liu, C.; Han, H.; Chen, K.; Li, W.; He, Q.; Peng, H.; Chen, J. Hierarchical Nanogaps within Bioscaffold Arrays as a High-Performance SERS Substrate for Animal Virus Biosensing. *ACS Appl. Mater. Interfaces* **2014**, *6*, 6281−6289.

(37) Pine, A. S.; Dresselhaus, G. Raman Spectra and Lattice Dynamics of Tellurium. *Phys. Rev. B* **1971**, *4*, 356−371.

(38) Narayanan, R.; Sarkar, D.; Som, A.; Wleklinski, M.; Cooks, G. R.; Pradeep, T. Anisotropic Molecular Ionization at 1 V from Tellurium Nanowires (Te NWs). *Anal. Chem.* **2015**, *87*, 10792−10798.

(39) Isomäki, H.; Boehm, J. Optical Absorption of Tellurium. *Phys. Scr.* **1982**, *25*, 801−803.

(40) Lin, Z.-H.; Yang, Z.; Chang, H.-T. Preparation of Fluorescent Tellurium Nanowires at Room Temperature. *Cryst. Growth Des.* **2008**, *8*, 351−357.

(41) Zhu, Y.; Wang, W.; Qi, R.; Hu, X. Microwave-Assisted Synthesis of Single-Crystalline Tellurium Nanorods and Nanowires in Ionic Liquids. *Angew. Chem.* **2004**, *116*, 1434−1438.

(42) Mohamed, M. B.; Ismail, K. Z.; Link, S.; El-Sayed, M. A. Thermal Reshaping of Gold Nanorods in Micelles. *J. Phys. Chem. B* **1998**, *102*, 9370−9374.

(43) Brioude, X. C. J. A.; Jiang, X. C.; Pileni, M. P. Optical Properties of Gold Nanorods: DDA Simulations Supported by Experiments. *J. Phys. Chem. B* **2005**, *109*, 13138−13142.